NACA RM L55L30b

NACA

RESEARCH MEMORANDUM

THEORETICAL PREDICTION OF THE SIDE FORCE ON STORES ATTACHED TO CONFIGURATIONS TRAVELING AT SUPERSONIC SPEEDS

By Percy J. Bobbitt, Frank S. Malvestuto, Jr., and Kenneth Margolis

Langley Aeronautical Laboratory
Langley Field, Va.

NATIONAL ADVISORY COMMITTEE FOR AERONAUTICS

WASHINGTON

March 12, 1956
Declassified December 8, 1961

NATIONAL ADVISORY COMMITTEE FOR AERONAUTICS

RESEARCH MEMORANDUM

THEORETICAL PREDICTION OF THE SIDE FORCE ON STORES ATTACHED TO CONFIGURATIONS TRAVELING AT SUPERSONIC SPEEDS

By Percy J. Bobbitt, Frank S. Malvestuto, Jr., and Kenneth Margolis

SUMMARY

Linear-theory evaluations of the important flow-field and interference effects necessary to the calculation of the store side forces have been illustrated and discussed. By taking into account these effects good agreement has been obtained between the theoretical predictions of the side force on the store and experimental values for the configurations examined. An appendix has been included which discusses the calculations and presents some of the equations necessary to obtain the flow-field and interference quantities.

INTRODUCTION

The aerodynamic forces and moments on stores and store-pylon arrangements situated below wings have in recent years been the subject of an intensive experimental effort. The effect on the store loads of store position, store size, pylon, wing plan form, and Mach number have all been investigated to varying degrees of thoroughness. Obviously, the general store problem has many variables. Although the complexity of the problem dictated that the initial approach be experimental, it also requires that an analytical or semiempirical method be developed to indicate trends, if not magnitudes, of the forces acting on the store when the many variables involved are changed. Subsonically, a good start toward this goal has been made by the National Advisory Committee for Aeronautics and the results were presented in reference 1.

The object of the present paper is to present some preliminary results of a study made to examine how well the aerodynamic forces acting on stores attached to configurations traveling at supersonic speeds may be predicted theoretically. The methods used to attack the problem are in general based on linearized theory and would naturally be expected to give the best results when the aircraft configurations are at small angles of attack and are composed of slender bodies and thin wings.

In the present paper the discussion is restricted to the lateral force component; however, the determination of the lift and drag forces on the store is amenable to the same type of theoretical treatment used to determine the side force.

SYMBOLS

C_Y	lateral-force coefficient, $\frac{\text{Side force on store}}{q \times \text{Frontal area of store}}$
α	angle of attack of wing
A	aspect ratio
M	Mach number
V	free-stream velocity
b	span
σ	sidewash angle in radians, approximately equal to $-\frac{v}{V}$
l	fuselage length
x	longitudinal distance
α_s	angle of attack of store
Y	lateral force on store in presence of reflection plane
Y_i	lateral force on isolated store
r	maximum store radius
s	distance from reflection plane to center of base
x_s	longitudinal distance from nose of store
l_s	length of store
v	sidewash or lateral velocity
q	free-stream dynamic pressure

$\beta = \sqrt{M^2 - 1}$

m tangent of wing semiapex angle

ϕ perturbation velocity potential

DISCUSSION

The presentation of data in the following section falls into three main categories: First, some of the basic flow fields necessary to the prediction of the store side forces are discussed; second, the interference effects between the wing or wing pylon and the store are analyzed; and lastly, the lateral forces acting on a store, calculated analytically, are compared with experimental values.

Figure 1 shows the wing-body-store arrangement used to illustrate some of the component flow fields. The triangular wing has a sweep of 60° and an aspect ratio of 2.31. The fuselage has a fineness ratio of 10, a near-parabolic nose shape, and a cylindrical afterbody. Subsequent flow-field variations are given at three spanwise stations of the wing shown in figure 1. These stations are at 0.25b/2, 0.50b/2, and 0.75b/2. The vertical distance below the wing at which the flow-field calculations were made is 0.10b/2.

Force calculations, which will be discussed later, have been made for the modified Douglas Aircraft Company (DAC) store shown in figure 1 attached to the triangular wing at the 0.50b/2 station. Exact dimensions of the DAC store and fuselage are given in reference 2.

Flow Fields

One of the more important flow-field effects is the sidewash produced by the wing at an angle of attack. A recent theoretical investigation of the angle-of-attack flow field has been made (see appendix) and a sampling of the results is shown in figure 2. This figure shows the chordwise variation of sidewash angularity below the wing at an angle of attack for two Mach numbers ($M = 1.6$ and $M = 2.1$). At a Mach number of 1.6, the leading edge of the wing is subsonic, that is, the Mach cone emanating from the wing-fuselage juncture is ahead of the leading edge; at a Mach number of 2.1, the wing leading edge is supersonic. It might be pointed out that the $-\sigma$ on the vertical scale indicates that the direction of the sidewash below the wing is from the wing root toward the wing tip.

The sidewash angularity due to the wing being at an angle of attack has a value of zero at the Mach cone emanating from the wing-root—fuselage juncture, rises rapidly to its maximum value at a longitudinal station just to the rear of the wing leading edge, and then decreases at a less rapid rate. Note that in going from the inboard to the outboard station there is a large increase in the magnitude of the induced angle of sidewash.

The main difference to be noted between the lateral angularity for the supersonic-edge Mach number shown on the right of figure 2 and that of the subsonic-edge condition is that, for the supersonic-edge case, the sidewash angularity has a constant value at all span stations in the region ahead of the Mach cone from the wing root that is followed by a rapid dropoff, whereas the maximum values increase spanwise for the subsonic-edge case. In the rearward portions of the wing there does not appear to be a significant difference between the sidewash-angularity magnitudes for the two Mach numbers shown. Lateral-angularity curves for Mach numbers other than those in figure 2 indicate appreciable differences in the magnitude of the sidewash in the rearward portion of the wing.

In addition to the angle-of-attack sidewash, other flow-field effects of importance are those due to fuselage thickness, wing thickness, and fuselage angle of attack. The fuselage angle-of-attack sidewash was found to be negligible at the points located $0.10b/2$ below the wing and at the three span stations considered. For other positions relative to the wing-fuselage, the fuselage angle-of-attack sidewash could have a significant effect so that each individual configuration must be considered separately.

Some illustrative chordwise variations of the sidewash angularity due to body thickness and wing thickness are shown in figure 3. The Mach number for these calculations is 1.6. It should be pointed out that the analyses from which the variations shown in figure 3 were taken (see appendix) apply for all supersonic Mach numbers and the Mach number of 1.6 was chosen because experimental force data were available at this Mach number.

The sidewash angularity due to body thickness has a value of zero at the Mach cone originating at the fuselage nose and rises rapidly to its maximum value. Behind a Mach line stemming from the end of the fuselage nose, the body-thickness sidewash angularity is negligible. Maximum values of the body-thickness angularities decrease as the distance from the body increases.

Sidewash angularity due to wing thickness (fig. 3) for a rhombic airfoil section has been plotted for wing thicknesses of 3 percent and 5 percent. The variations depicted are along the $0.50b/2$ station. It can be seen that regions of both positive and negative angularity occur and that, if a store were immersed in this sidewash field at various longitudinal positions, it would be subjected to both positive and negative resultant loads. Note that the magnitudes of the sidewash

angularity due to body thickness and that due to wing thickness are comparable (fig. 3).

Interference Effects

Several theoretical studies have been made to evaluate the induced effects of the wing and wing pylon on the store. (See appendix.) The theoretical wing-pylon-store model used in the interference calculations is shown in figure 4. What is referred to herein as the wing is actually an infinite wing or reflection plane at an angle of attack of 0°. The store in one analysis has been connected to the wing with a pylon and in another it has not. The analyses allow the store to be placed at small angles of incidence to the free stream. A positive store incidence angle is the case where the store nose has been moved toward the wing. In the analyses the store or store pylon has been placed in a uniform sidewash field as indicated by the arrows. This sidewash field causes a side force on the store and it is the effect of the wing and pylon on this side force that is of interest.

The left-hand part of figure 5 has been presented to illustrate the effect of the wing interference on the side force on the store where the store is not connected with a pylon. The plot on the right-hand side shows the pylon effect. It can be seen in the left-hand plot that both a decrease in the distance of the store from the wing and a positive increase in the store angle of attack cause an increase in the side force on the store. When a pylon is added to the system (right-hand plot of fig. 5), there is a large change in the induced load on the store in the direction to increase the side force on the store.

Side-Force Distribution on Store

The discussion until now has been related to the more important flow-field and interference effects. In order to depict how the side force will distribute itself along a store when it is immersed in the various sidewash fields and subject to the wing interference, figure 6 has been prepared. Figure 6 shows the side-force distribution on the DAC store located at the $0.50b/2$ station under the 60° swept delta wing. The wing-body-store configuration is at an angle of attack of 6°. It can be noted that the resultant side force on the store is directed from the wing root toward the wing tip and also that, if moments were taken about the store midpoint, they would be in the direction tending to push the nose of the store out toward the wing tip.

Store Side-Force Correlations

With the theoretical raw materials discussed in the previous sections, side-force-coefficient calculations have been made for the DAC store located in various positions beneath swept, unswept, and delta wings. Figures 7 and 8 show correlations for the store located below the delta wing and figures 9 and 10, correlations for the unswept and swept wings. The experimental values shown on these figures have been obtained from references 3 and 4. All correlations are at a Mach number of approximately 1.6.

In figure 7 the effect of store lateral location and angle of attack on the store side-force coefficient for the 60° delta-wing configuration is shown. The store beneath the wing in this figure is not connected with a pylon. Two spanwise locations (0.50b/2 and 0.85b/2) have been considered. Note that there is a large increase in the side-force coefficient when the store is moved from the midspan to the tip location. This increase is primarily due to the larger magnitude of the angle-of-attack sidewash in the tip region which is illustrated in figure 2. The agreement between the theoretical predictions and experiment is good for both lateral locations.

The effect of longitudinal store position on the side force on the store located beneath the same 60° delta wing as that of figure 7 has been depicted in figure 8. When the store is moved from its location beneath the rear portion of the wing toward the leading edge, figure 8 shows that the store experiences a large increase in side force. Agreement between the theoretical predictions and experiment is good for both locations of the store considered.

It might be mentioned in connection with figure 8 that the upsweep of the experimental side-force-coefficient curve with increasing α is characteristic of the experimental side-force variations with α for stores situated beneath wings of most all plan forms. Static-force tests on the isolated store show a similar upsweep as the store angle of attack is increased. This fact would seem to indicate that, if in the theoretical calculations the crossflow viscous effects of Allen were taken into account, better agreement between the theory and experiment would be obtained at the moderate angles of attack.

Figure 9 shows the effect of spanwise store location on the side force on the store located under an unswept wing of aspect ratio 4. An extremely short pylon connects the store to the wing (see ref. 3) in both locations treated (0.47b/2 and 0.80b/2). It can be seen that the increase in the side-force coefficient experienced when the store is moved toward the wing tip is acceptably predicted by the theory.

The effect of a pylon on the side force on a store under a 45° swept wing of aspect ratio 4 is shown in figure 10. The lower two curves are for the pylon-off configuration and the upper two curves, for the pylon-on case. The agreement between theory and experiment for both conditions is good.

A note of caution is in order. The agreement obtained between the theoretical predictions of the side force on the DAC store and experiment shown in figures 7 to 10 may be fortuitous to some extent. The fact that the store has a finite base could have benefited the agreement since, as is well known, linearized theory predicts an unrealistic zero lift force on closed bodies of revolution at an angle of attack in a uniform stream. It is possible that experimental force data on the isolated store could be used together with the theoretical flow fields and interference effects to give reliable estimates of the side force on stores of almost all shapes. The limitations of the pure theoretical approach can not be defined until more correlations between theory and experiment such as those presented herein have been made.

CONCLUSIONS

In conclusion, it may be said that the important flow-field and interference effects can be calculated by theory and that, by taking into account these flow-field and interference effects, good agreement has been obtained between the theoretical predictions of the side force on the store and experimental values for the configurations examined. Although the application of theory in this paper has been specialized primarily to side force on the store, indications are that the other aerodynamic forces are also amenable to this same type of theoretical treatment.

An appendix has been included which discusses the calculations and presents some of the equations necessary to obtain the flow-field and interference quantities.

Langley Aeronautical Laboratory,
National Advisory Committee for Aeronautics,
Langley Field, Va., November 1, 1955.

APPENDIX

REMARKS AND EQUATIONS PERTAINING TO THE CALCULATION OF FLOW FIELDS, INTERFERENCE EFFECTS, AND STORE SIDE FORCES

In the text some illustrative flow-field variations, interference effects, and store side forces have been discussed with no indication given as to how they were obtained. The methods used in the evaluation of several of these effects are well known and only a few remarks are needed to make clear the procedure, whereas for others useful equations can be presented and discussed. More extensive treatments of some of the effects have been made at the Langley Aeronautical Laboratory than indicated in the following sections; however, the limited objectives of the present paper obviate the need for more detailed descriptions herein.

Angle-of-Attack Sidewash

From a procedure paralleling that used by Nielsen and Perkins in reference 5 to determine the downwash in the flow field exterior to flat lifting triangles of infinite chord, the sidewash or lateral flow below this same lifting wing has been obtained. The analyses apply for all leading-edge sweeps and supersonic Mach numbers, both the subsonic-wing leading-edge and supersonic-wing leading-edge conditions being considered. The equation for the sidewash below the wing at a point (x,y,z) for the subsonic-edge case is given by

$$v = \frac{V\alpha}{\left(1 - s_o^2\right)E\left(\sqrt{1 - \beta^2 m^2}\right)}\left\{-E\left(\sqrt{\sigma_1}, s_o^2\right) + \frac{\left[1 - \left(1 - s_o^4\right)\lambda_1\right]\sqrt{\sigma_1}\sqrt{1 - \sigma_1}\sqrt{1 - s_o^4\sigma_1}}{1 - \left[1 - \left(1 - s_o^4\right)\lambda_1\right]\sigma_1} + E\left(\sqrt{\sigma_2}, s_o^2\right) - \frac{\left[1 - \left(1 - s_o^4\right)\lambda_2\right]\sqrt{\sigma_2}\sqrt{1 - \sigma_2}\sqrt{1 - s_o^4\sigma_2}}{1 - \left[1 - \left(1 - s_o^4\right)\lambda_2\right]\sigma_2}\right\} \tag{A1}$$

where

$$s_o = \frac{1 - \sqrt{1 - \beta^2 m^2}}{\beta m}$$

The procedure for calculating the λ and σ functions is straightforward and requires just a few steps although the calculations themselves are a little lengthy. First calculate p and q:

$$p = \frac{\beta \frac{z}{x}}{1 + \sqrt{1 - \left(\beta \frac{y}{x}\right)^2 - \left(\beta \frac{z}{x}\right)^2}} \tag{A2}$$

$$q = \frac{\beta \frac{y}{x}}{1 + \sqrt{1 - \left(\beta \frac{y}{x}\right)^2 - \left(\beta \frac{z}{x}\right)^2}} \tag{A3}$$

and then τ_1, δ_1, τ_2, and δ_2:

$$\tau_1 = \left[p\sqrt{\sqrt{\left(p^2 - q^2 + s_o^2\right)^2 + 4p^2q^2} + p^2 - q^2 + s_o^2} + q\sqrt{\sqrt{\left(p^2 - q^2 + s_o^2\right)^2 + 4p^2q^2} - \left(p^2 - q^2 + s_o^2\right)} \right] \frac{1}{\sqrt{2}\sqrt{\left(p^2 - q^2 + s_o^2\right)^2 + 4p^2q^2}} \tag{A4}$$

$$\delta_1 = \left[-p\sqrt{\sqrt{\left(p^2 - q^2 + s_o^2\right)^2 + 4p^2q^2} - \left(p^2 - q^2 + s_o^2\right)} + q\sqrt{\sqrt{\left(p^2 - q^2 + s_o^2\right)^2 + 4p^2q^2} + p^2 - q^2 + s_o^2} \right] \frac{1}{\sqrt{2}\sqrt{\left(p^2 - q^2 + s_o^2\right)^2 + 4p^2q^2}} \tag{A5}$$

$$\tau_2 = \frac{\sqrt{\sqrt{\left[1 + s_o^2(p^2 - q^2)\right]^2 + 4s_o^4p^2q^2} + 1 + s_o^2(p^2 - q^2)}}{\sqrt{2}\sqrt{\left[1 + s_o^2(p^2 - q^2)\right]^2 + 4s_o^4p^2q^2}} \tag{A6}$$

$$\delta_2 = \frac{-\sqrt{\sqrt{\left[1 + s_o^2(p^2 - q^2)\right]^2 + 4s_o^4p^2q^2} - \left[1 + s_o^2(p^2 - q^2)\right]}}{\sqrt{2}\sqrt{\left[1 + s_o^2(p^2 - q^2)\right]^2 + 4s_o^4p^2q^2}} \tag{A7}$$

Substitute τ_1 and δ_1 in the following two equations to determine λ_1 and σ_1 and substitute τ_2 and δ_2, to obtain λ_2 and σ_2.

$$\lambda = \frac{\left[(1 + \tau^2 + \delta^2) - \sqrt{(1 + \tau^2 + \delta^2)^2 - 4\tau^2}\right]\left\{1 + (1 - s_o^4)(\tau^2 + \delta^2) - \sqrt{\left[1 + (1 - s_o^4)(\tau^2 + \delta^2)\right]^2 - 4(1 - s_o^4)\tau^2}\right\}}{4(1 - s_o^4)\tau^2} \tag{A8}$$

$$\sigma = \frac{\tau^2 + \delta^2 - \lambda}{(\tau^2 + \delta^2 - \lambda) - \left[\lambda(1 - s_o^4)(\tau^2 + \delta^2) - 1\right]} \tag{A9}$$

The elliptic functions $E\left(\sqrt{\sigma}, s_o^2\right)$ and $E\left(\sqrt{1 - \beta^2m^2}\right)$ in the expression for v (eq. (A1)) may be obtained from tables (refs. 6 and 7) or by series expansion.

The equation for the sidewash in the region below the wing and behind the Mach cone emanating from the wing apex when the wing leading edge is supersonic is

$$v = \frac{V\alpha}{\pi\sqrt{\beta^2m^2 - 1}}\left[\tan^{-1}\frac{1 + \beta^2m\,\frac{y}{x}}{\sqrt{\beta^2m^2 - 1}\sqrt{1 - \left(\beta\,\frac{y}{x}\right)^2 - \left(\beta\,\frac{z}{x}\right)^2}} - \tan^{-1}\frac{1 - \beta^2m\,\frac{y}{x}}{\sqrt{\beta^2m^2 - 1}\sqrt{1 - \left(\beta\,\frac{y}{x}\right)^2 - \left(\beta\,\frac{z}{x}\right)^2}}\right] \tag{A10}$$

Sidewash in the region behind the plane Mach wave off the wing leading edge and ahead of the Mach cone from the wing apex is

$$v = \frac{V\alpha}{\sqrt{\beta^2m^2 - 1}} \tag{A11}$$

For the sonic-edge wing the sidewash expressions simplify to

$$v_{\beta m=1} = \frac{2V\alpha\beta\,\frac{y}{x}\sqrt{1 - \left(\beta\,\frac{y}{x}\right)^2 - \left(\beta\,\frac{z}{x}\right)^2}}{\pi\left[1 - \left(\beta\,\frac{y}{x}\right)^2\right]} \tag{A12}$$

It should be pointed out that, although the expressions given herein apply directly to determining the angle-of-attack sidewash below the infinite-chord triangular wing, they may also be used directly in sidewash determinations for some regions below wings having finite taper and chord. This is a rather simple point but one so often overlooked that a few additional remarks concerning it may be useful.

Consider an infinite-chord triangular wing and a conventional wing (see sketch), both having the same leading-edge sweep and both traveling at the same velocity.

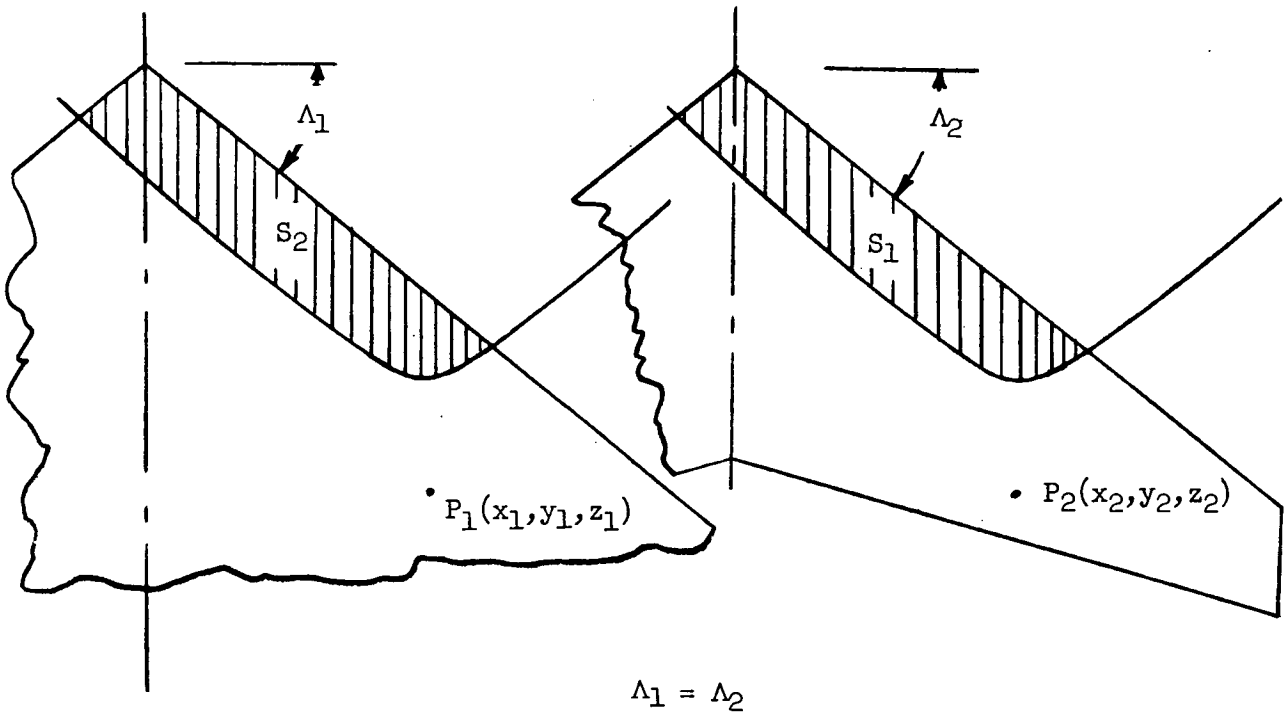

$$\Lambda_1 = \Lambda_2$$

$$S_1 = S_2$$

Points P_1 and P_2 below these wings are in the same position with respect to the wing leading edges and root chords so that forecones from these points cut off equal areas, S_1 and S_2, of the wing. Since the loadings in the two areas are the same, the flow fields at the points P_1 and P_2 are the same. For points the forecones of which intersect the tip of a wing or the wake behind a wing, additional considerations are, of course, necessary and the expressions for the sidewash velocity given here do not apply.

Sidewash Field Due to Body Thickness

The potential in space at a point (x,y) due to an axial distribution of sources is (ref. 8)

$$\phi = -\frac{V}{2\pi}\int_0^{x-\beta r} \frac{f_0(\xi)d\xi}{\sqrt{(x-\xi)^2 - \beta^2 r^2}} \tag{A13}$$

where $f_0(\xi)$ represents the source strength function, r is the radial distance from the x-axis to the field point at which the potential is desired, ξ is the longitudinal distance to each individual source, and x is the longitudinal distance to the field point at which the potential is desired. This equation is not often used in the form shown because of the difficulty involved in obtaining the $f_0(\xi)$ function and because interest is generally limited to the potential (or one of its derivatives) on the body surface where the expression for ϕ may be simplified and the distribution function can be approximated with a fair degree of accuracy. The problem at hand, however, does not allow the conveniences available when only the region in the vicinity of the body boundary is considered and some attempt must be made to approximate the $f_0(\xi)$ function for use in equation (A13).

It was found convenient to obtain the distribution function for the fuselage shown in figure 1 (see ref. 2 for dimensional detail) for a free-stream Mach number of 1.6 by utilizing the small r or slender-body distribution function as a starting point. First, an expression for $\partial\phi/\partial r$ is equal to the radial perturbation velocity as given by

$$\frac{\partial\phi}{\partial r} = \frac{V}{2\pi r}\int_0^{x-\beta r} \frac{f_0'(\xi)(x-\xi)d\xi}{\sqrt{(x-\xi)^2 - \beta^2 r^2}} \tag{A14}$$

was determined analytically by assuming the fuselage nose shape to be parabolic (a very close approximation to the actual nose shape) and by using the small r distribution function associated with this shape. Calculations were then made to obtain $\partial\phi/\partial r$ at points on the surface of the actual fuselage including the cylindrical part so that it could be determined how much the calculated flow differed from the required tangential flow, that is, a comparison of $\left(\frac{\frac{\partial\phi}{\partial r}}{V}\right)_{surface}$ and $\left(\frac{dr}{dx}\right)_{surface}$ was made. Differences between $\left(\frac{\frac{\partial\phi}{\partial r}}{V}\right)_{surface}$ and $\left(\frac{dr}{dx}\right)_{surface}$ indicated

that certain changes were necessary in the distribution function. Four distribution functions were tried before an acceptable one was found.

The sidewash at a point in the field is, of course, the radial velocity $\partial\phi/\partial r$ at that point multiplied by the cosine of the angle it makes with the horizontal.

Calculations of Sidewash Due to Wing Thickness

The calculation of the lateral-flow component requires the determination of the perturbation velocity $\partial\phi/\partial y$. The general expression for the linearized perturbation velocity potential in space due to wing thickness is

$$\phi(x,y,z) = -\frac{V}{\pi}\iint_R \frac{\lambda(\xi,\eta)d\xi\, d\eta}{\sqrt{(x-\xi)^2 - \beta^2(y-\eta)^2 - \beta^2 z^2}} \tag{A15}$$

where x, y, and z are the rectangular coordinates of the field point (that is, the point at which the potential is desired) and ξ and η are the rectangular coordinates (analogous to x and y) for the sources and sinks which are distributed in the $z = 0$ plane. The source-distribution function $\lambda(\xi,\eta)$ is related to the particular thickness distribution involved and is given as

$$\lambda(\xi,\eta) = \left[\frac{\partial}{\partial\xi} z(\xi,\eta)\right]_{z=0}$$

The integration is performed over the region R that is enclosed by the traces in the $z = 0$ plane of the Mach forecone emanating from the point (x,y,z) and by the wing plan-form boundaries. Differentiation of equation (A15) with respect to y will then yield the required lateral component $\partial\phi/\partial y$. The differentiation may, of course, be done after obtaining the potential or by suitable differentiation under the integral sign in either the initial or intermediate stages of integration.

With regard to carrying out the details of the calculation, some remarks are in order. If the distribution function $\lambda(\zeta,\eta)$ is continuous, the double integration may be analytically performed directly or if the resulting integrals are difficult to handle, a straightforward numerical procedure can be employed. On the other hand, if the distribution function $\lambda(\xi,\eta)$ is discontinuous, as is the situation for a multiwedge-type

surface, the numerical procedures probably constitute the most efficient methods of solution. In this connection, however, it should be pointed out that superposition of simple wedge-type distributions to build up the desired distribution simplifies the calculations considerably in many cases and even enables analytical solutions to be obtained more readily.

Side Force Acting on a Slender Store in the Presence of an Infinite Wing at Zero Angle of Attack

The following expression for the side force Y acting on a store situated below an infinite wing (fig. 4) was evolved from a slender-body-theory analysis. The side-force expression is independent of Mach number and therefore is only a rough estimate of the side force at Mach numbers where strong shock interactions occur between the store and the reflection plane.

In coefficient form, the side-force expression is

$$C_Y = \frac{Y}{qS} = -2\beta H\left(\xi_\beta\right) + \frac{2\alpha_s\beta}{S}\int_0^l \pi r(x)\,\frac{dH(x)}{dx}\,\frac{dx}{d\xi}\,dx \tag{A16}$$

where

x axial coordinate of store

$r(x)$ local radius of store

$S(x) = \pi r^2(x)$

$S'(x) = \dfrac{dS(x)}{dx}$

S base area

l length of store

s distance of store axis at base from infinite wing

$\xi = \dfrac{s - \alpha_s(l - x)}{r(x)}$; ξ_β is value of ξ at base

$$\frac{dx}{d\xi} = -\frac{r^2(x)}{\left[s - \alpha_s(l - x)\right]\frac{dr(x)}{dx} + \alpha_s r(x)} = -\frac{r(x)}{\xi\frac{dr(x)}{dx} - \alpha_s}$$

The $H(x)$ function and its derivative $\frac{dH(x)}{dx}$ are defined compactly in terms of the elliptic nome q

$$H(q) = 1 + 2\sum_{m=1}^{m=\infty}\frac{(1 - q)^2 q^m}{\left(1 - q^{m+1}\right)^2} \tag{A17}$$

$$\frac{dH(x)}{dx} = \frac{dH(q)}{dq}\frac{dq}{d\xi}\frac{d\xi}{dx}$$

$$= -8\frac{d\xi}{dx}\sum_{m=1}^{m=\infty}\frac{q^{m+\frac{1}{2}}}{\left(1 - q^{m+1}\right)^3}\left[m - (m + 2)q + (m + 2)q^{m+1} - mq^{m+2}\right] \tag{A18}$$

where

$$q = \frac{1}{\left(\xi + \sqrt{\xi^2 - 1}\right)^2}$$

$$\frac{dq}{d\xi} = -\frac{2}{\left(\xi + \sqrt{\xi^2 - 1}\right)^2\sqrt{\xi^2 - 1}}$$

For small values of q (order of 0.1) only three or four terms of the expansion are necessary whereas for larger values of q (order of 0.5 or 0.6) as many as 13 or 14 terms may be required.

The Interference Effect of a Pylon and Infinite Wing on the Side Force on a Store

The problem of determining the side force of stores connected to wings with pylons is similar in some respects to the problem of determining the lift force on wing-tip tanks. Recognizing this, the transformation procedures of reference 9, which treat wing-tip tanks, have been incorporated in an analysis paralleling that of the previous section to compute side forces on stores attached to an infinite wing with a pylon. Compact expressions for the store side force, like those of the previous section, are not possible for the pylon case. The involved nature of the calculative procedure for obtaining the store side force prevents a more detailed description in this paper.

It should be pointed out here as in the previous section that, when strong shock interactions between the store and wing are present, the applicability of a subsonic crossflow analysis is questionable.

Store Side Force

The determination of the side force and moments acting on the store situated under the right wing panel and immersed in the various sidewash fields requires a knowledge of the pressure difference across the store which, in turn, requires a knowledge of the perturbation velocities on the store surface. The equation for the perturbation velocity potential from which the perturbation velocities have been derived (ref. 8) is

$$\phi = \frac{V \cos \theta}{2\pi r} \int_0^{x-\beta r} \frac{f_1'(\xi)(x - \xi)d\xi}{\sqrt{(x - \xi)^2 - \beta^2 r^2}} \tag{A19}$$

where the distribution function $f_1'(\xi)$ for a slender body of revolution immersed in a uniform lateral field is

$$f_1'(\xi) = -2\sigma S(x)$$

The angle θ in equation (A19) is measured clockwise from the horizontal. The symbols x, ξ, and r are defined in the section entitled "Calculation of Sidewash Due to Wing Thickness." Since the store lies in a nonuniform sidewash field, the change in the induced lateral angle of incidence along the store should be accounted for to obtain the correct results. In the calculations made for the Douglas store, it has been assumed that the

effect of the change in incidence along the store could be accounted for by allowing σ in the distribution function to vary with ξ

$$f_1(\xi) = -2\sigma(\xi)S(\xi)$$

The integrations necessary to obtain ϕ or one of its derivatives must be solved numerically. It is expedient in most cases to perform a parts integration prior to doing the numerical integrations to eliminate the square root in the denominator.

REFERENCES

1. Alford, William J., Jr.: Effects of Wing-Fuselage Flow Fields on Missile Loads at Subsonic Speeds. NACA RM L55E10a, 1955.

2. Jacobsen, Carl R.: Effects of the Spanwise, Chordwise, and Vertical Location of an External Store on the Aerodynamic Characteristics of a 60° Delta Wing at Mach Numbers of 1.41, 1.62, and 1.96. NACA RM L52H29, 1952.

3. Guy, Lawrence D.: Loads on External Stores at Transonic and Supersonic Speeds. NACA RM L55E13b, 1955.

4. Smith, Norman F., and Carlson, Harry W.: Some Effects of Configuration Variables on Store Loads at Supersonic Speeds. NACA RM L55E05, 1955.

5. Nielsen, Jack N., and Perkins, Edward W.: Charts for the Conical Part of the Downwash Field of Swept Wings at Supersonic Speeds. NACA TN 1780, 1948.

6. Jahnke, Eugene, and Emde, Fritz: Tables of Functions. Fourth ed., Dover Publications, 1945.

7. Byrd, Paul F., and Friedman, Morris D.: Handbook of Elliptic Integrals for Engineers and Physicists. Lange, Maxwell & Springer, Ltd. (New York), 1954.

8. Ferri, Antonio: Elements of Aerodynamics of Supersonic Flows. The Macmillan Co., 1949.

9. Hartley, D. E.: Theoretical Load Distributions on Wings With Tip-Tanks. Rep. No. Aero. 2469, British R.A.E., June 1952.

WING-BODY-STORE ARRANGEMENT
WING SWEEP 60°; BODY FINENESS RATIO 10

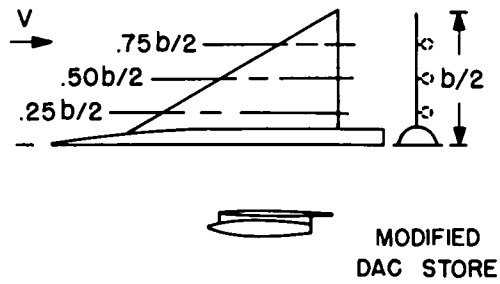

Figure 1

CHORDWISE VARIATION OF SIDEWASH ANGULARITY
DUE TO WING AT ANGLE OF ATTACK

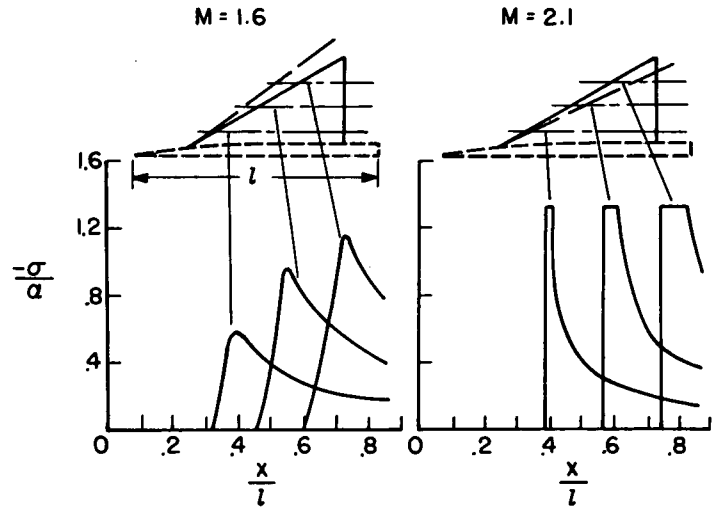

Figure 2

CHORDWISE VARIATIONS OF SIDEWASH ANGULARITY DUE TO BODY AND WING THICKNESS

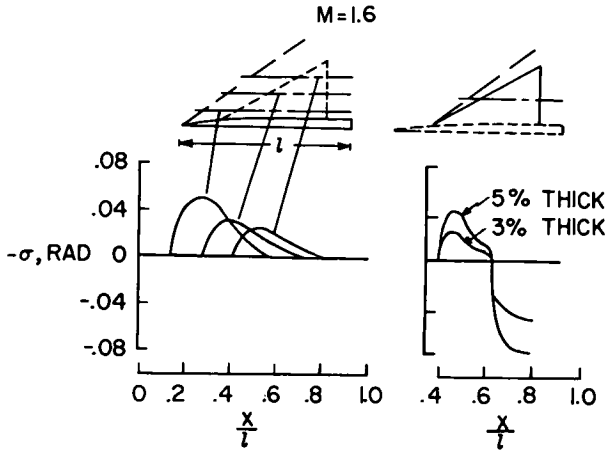

Figure 3

INFINITE WING-PYLON-STORE CONFIGURATION USED TO ILLUSTRATE INTERFERENCE CALCULATIONS

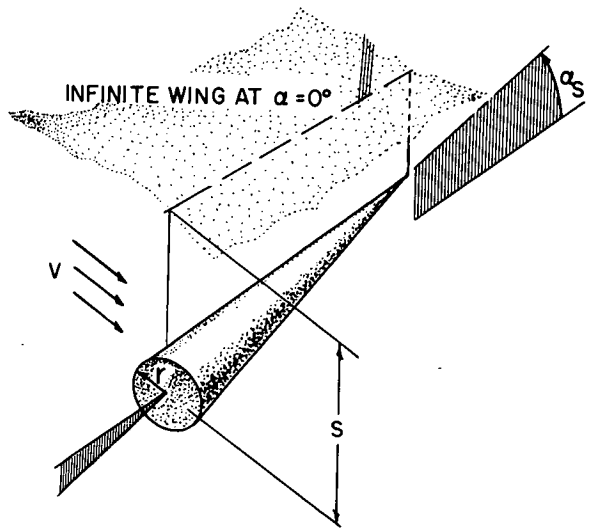

Figure 4

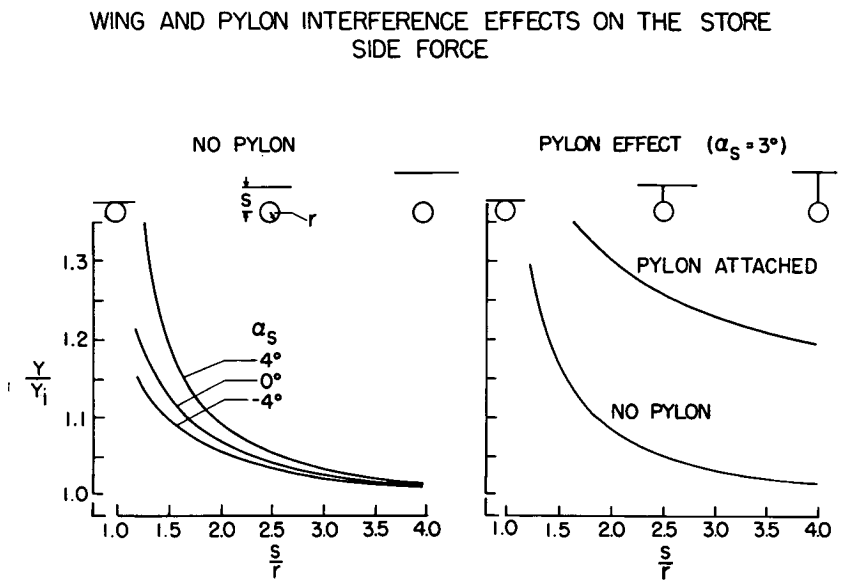

Figure 5

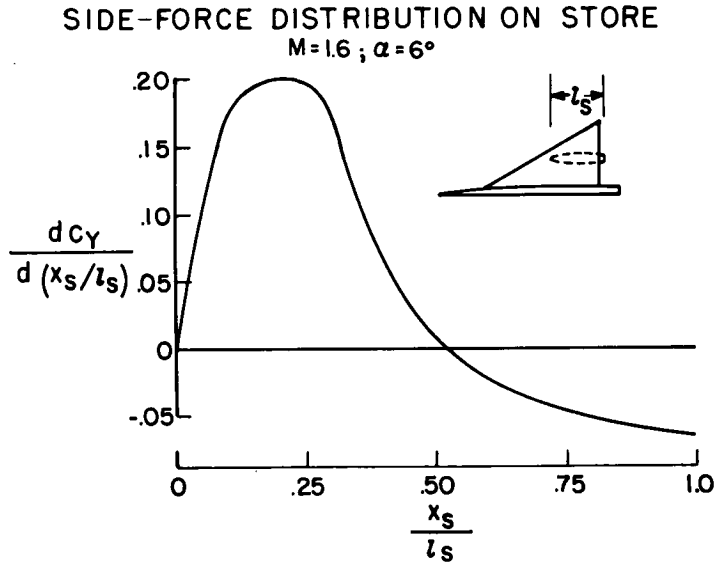

Figure 6

EFFECT OF STORE LATERAL LOCATION AND ANGLE OF ATTACK ON C_Y (NO PYLON)

M≈1.6

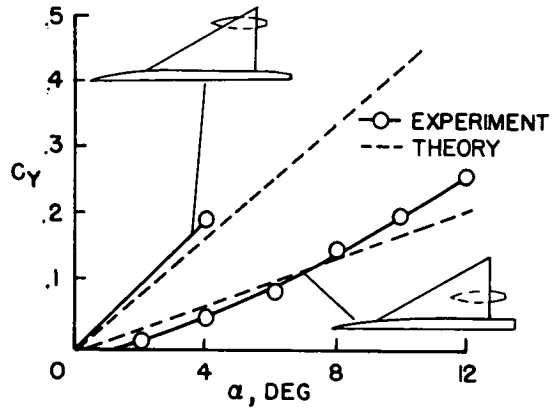

Figure 7

EFFECT OF LONGITUDINAL STORE POSITION ON THE SIDEFORCE ON STORE UNDER 60° DELTA WING (PYLON ATTACHED)

M ≈ 1.6

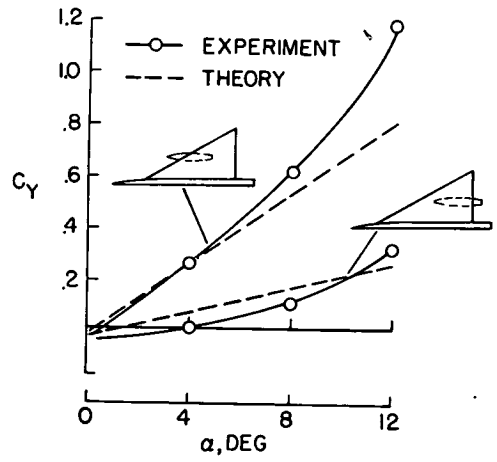

Figure 8

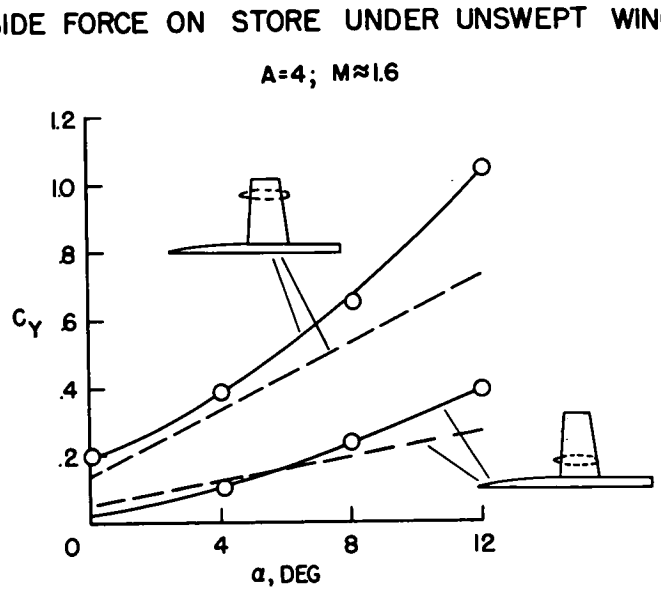

Figure 9

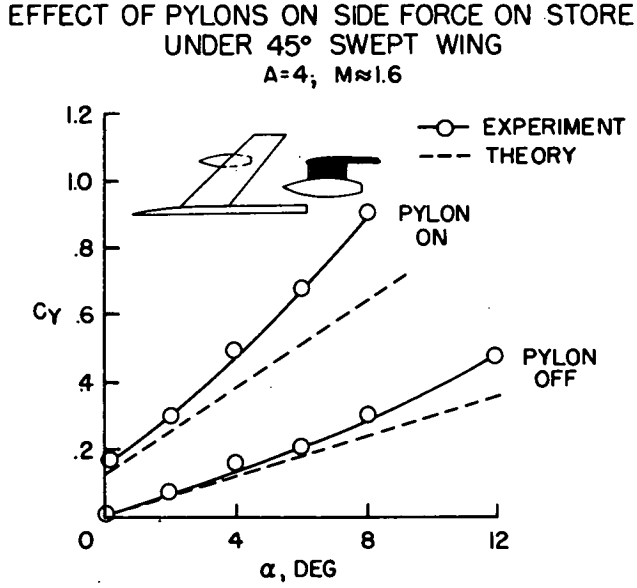

Figure 10